Modeling and Characterization of Downwind Tower Shadow Effects using a Wind Turbine Emulator

Modeling and Characterization of Downwind Tower Shadow Effects using a Wind Turbine Emulator

Leong Kit Gan, Jonathan K. H. Shek, *Member, IEEE*, Markus A. Mueller

***Abstract*— This paper presents the modeling and characterization of the tower shadow effects using a wind turbine emulator in a laboratory environment. In particular, the downwind wind turbines are considered here as their tower shadow effects are more significant compared to the upwind counterpart. Simulation and experimental results have shown that the wind speed deficit due to this non-ideal effect is significant. In addition, the tower shadow effects occur typically two to three times per revolution, depending on the number of blades. The modeling of the tower shadow profiles for tubular and four-leg tower configurations are presented. Typically, these towers are used in small wind turbine applications. The tower shadow profiles are emulated experimentally using a wind turbine emulator with its characteristics being explained. The limitations of emulating the tower shadow effects using a wind turbine emulator are demonstrated through the frequency response test performed in this work. In this research, the wind turbine emulator is connected to an isolated grid which is formed by three single-phase inverters. Finally, the paper concludes with a sensitivity analysis of the power oscillations for different widths and magnitudes of the tower shadow profile.**

***Index Terms*—downwind tower shadow, wind turbine emulator, off-grid, isolated, renewable energy, experiment, modeling, frequency response**

I. INTRODUCTION

WIND energy has attracted worldwide attention for electric power generation due to the global environmental concerns associated with fossil energy resources [1]. Wind energy is believed as a promising and encouraging renewable energy for the power generation industry as it is the fastest growing source to meet the renewable targets in many countries [2]. However, wind energy sources are intermittent in nature and site specific. In addition, a pulsating wind turbine torque is produced when the wind turbine blade passes its tower. As a result, the power quality in the grid is greatly affected as there has been an extensive growth in quantity in the exploitation of wind energy nowadays [3]. In the past, many wind turbine related studies have been focusing on large-scale and grid-connected wind turbines, and little attention has been given to decentralized small-scale wind turbines. The latter is often viewed as a socio-economically viable solution for most developing countries, where grid connection is a challenge [4].

For horizontal axis wind turbines, the rotor orientation may be either upwind or downwind. Following the wind direction, the former has the rotor in front of the tower, whereas the latter has the rotor behind the tower whereby the blades rotate through the disturbed air produced by the tower's aerodynamic shadow. The upwind rotor requires stiffer blades because the wind may bend the rotor towards the tower. Due to this reason, the rotor weight is often increased which could lead to an increase in load applied to the bearing and the tower. In addition, an active yaw mechanism is essential to keep the rotor facing the wind. For wind turbines with downwind configuration, the centrifugal forces which tend to counteract moments due to thrust reduce the blade root flap bending moments [5]. A significant advantage of the downwind wind turbine is that the rotor blades may bend at high wind speeds and therefore reducing the loading effect on the tower [6]. However, the tower produces a wake in the downwind direction, and the blades must pass through that wake every revolution. This pressure fluctuation of airflow is a source of periodic loads which may impose a high fatigue load on the blades and propagate the ripple on the electrical power produced. This phenomenon is known as 'tower shadow'. Although this effect is more significant in the downwind configuration, tower shadow occurrence in the upwind configuration is also apparent.

On an upwind wind turbine, the perturbation of the flow is caused by a redirection of the incoming flow due to the presence of the tower. As such, the tower shadow on the upwind turbines is not very severe, and it gives rise to a quasi-steady aerodynamic response on the blades. On a downwind turbine, the rotor passes the highly unsteady airflow as a result of high Reynolds number flow over the circular cylinders [7]. Two effects therefore dominate the interaction between the blades and the wake (caused by the tower). First, the presence of tower that creates a velocity deficit can cause the blade to experience a sudden drop in wind speed when it travels through the wake. Secondly, the blade could occasionally

Manuscript received May 20, 2016; revised September 28, 2016, November 8, 2016 and January 15, 2017; accepted March 9, 2017. This work is supported in part by the Commonwealth Scholarship Commission – United Kingdom and in part by The University of Edinburgh.

L. K. Gan is with the Department of Engineering Science, University of Oxford, Oxford, OX1 3PJ, U. K. (e-mail: leong.gan@eng.ox.ac.uk).
J. K. H. Shek and M. A. Mueller are with the Institute for Energy Systems, The University of Edinburgh, Edinburgh, EH9 3DW, UK. (e-mail: J.Shek@ed.ac.uk; Markus.Mueller@ed.ac.uk).

encounter the vortices which are shed from the tower. It is reported from the literature that the peak-to-mean torque variation is about 6% to 12% for the upwind cases and 24% to 38% for the downwind cases, regardless of the number of blades and the rotor speed [6].

The tower shadow effect may cause flicker, degrading the power quality at grid level. As a result, the illumination intensity of light sources can be affected and it provides unpleasant visual sensation among utility customers. Even at the scale of a wind farm, it was demonstrated that the flicker effect is more severe if the wind turbines are synchronized in operation [8]. From a research point of view, the flicker phenomenon is mostly studied at wind farm level, and they are grid-connected. In an off-grid hybrid system which consists of battery storage and diesel generators as backup, the harmonics generated from the tower shadow effect can be propagated to them and eventually reducing their lifetime. It is acknowledged that flicker presents one of the most complex testing procedure compared to other power quality disturbances [9]. Besides, it is costly and challenging to study only the tower shadow effect in the field due to the difficulty of isolating it from other non-ideal effects (for instance the wind shear and turbulence effect). Also, repeatability tests cannot be carried out as a constant wind speed is hardly achievable for the required time frame.

With the proposed methodology of emulating the tower shadow profiles in the laboratory environment, wind turbine manufacturers and researchers can study the contribution of tower shadow effect on the flicker problem. The propagation of the tower shadow effect is demonstrated at different stages within the wind turbine emulator. The analysis elaborated in this paper includes the limitations and considerations involved when developing a realistic wind turbine emulator. It is important to note that although the investigation of tower shadow effect is formulated based on a small fixed-speed wind turbine in an isolated scenario, the analysis is generic and it is suitable to be adopted by both fixed-speed and variable-speed wind turbine technologies at various scales. One of the main differences between the fixed-speed and variable-speed wind turbines is the presence of power electronics interface between the generator and the grid for the latter. The variable speed operation can potentially mitigate this problem with the support from some storage elements such as capacitors or supercapacitors. Nevertheless, the generator which is directly coupled to the rotor blades will still be producing power with oscillations as a result of the tower shadow effects. The modeling approach and analysis carried out can serve as a reference and can be modified to suit any other systems of interest.

In [10], Dale presented an analytical formulation of the aerodynamic torque for a three-bladed upwind wind turbine, which includes the effects of wind shear and tower shadow. The model was developed as an input function of turbine-specific parameters such as the radius, height, tower dimensions, as well as the site parameter (wind shear exponent). The main advantage of this model is that it is suitable for time-domain simulation. It was formulated based on an "equivalent wind speed" which has been developed by Sørensen [11]. Dale's simulation studies found that much larger tower-shadow-induced oscillations mask the presence of wind-shear-induced 3p oscillations. It contributes to approximately a 1% DC reduction in average torque [10]. This work was then adopted by [12] to characterize the presence of shaft speed ripples in wind turbines as a result of wind shear and tower shadow. The derived conclusion was that the relative amount of shaft speed ripples caused by wind shear and tower shadow is independent of the turbine size [12]. The authors in [13] and [14] brought forward Dale's equivalent wind speed model in studying the impact of wind shear and tower shadow on wind farms and large-scale grid-connected wind power systems. A variable speed wind turbine emulator was successfully developed with the incorporation of Dale's equivalent wind speed model [15]. Experimental results showed that wind shear and tower shadow can be emulated in a laboratory environment [15]. More recently, the authors in [16] have integrated Dale's model and a generic yaw error model to investigate the effects of yaw error on wind turbine running characteristics at different stages of operation. Interestingly, the literature demonstrated in simulation that the yaw errors can restrain the 3p torque pulsation. This restraining effect became more severe as the yaw error increases [16]. In literature [17], the mechanical and aerodynamic aspects of the wind turbine system were simulated and the effects of tower shadow, wind shear, yaw error and turbulence on the power quality of a wind-diesel system were shown individually. Others such as [18] and [19] represented the tower shadow effect as cosine waveform with an empirical coefficient. This approach reduces the modeling complexity, but the accuracy and the correctness have yet to be characterized against other analytical models.

This paper presents in the following structure. Firstly, the modeling of downwind tower shadow effects is described in Section II. These include tubular and four-leg tower configurations. Section III discusses the limitations and the characterization of the tower shadow profile using a wind turbine emulator. Using the developed hybrid system setup, a sensitivity analysis of the power oscillations for different widths and magnitudes of the tower shadow profile is also carried out. Finally, conclusions derived from the research are summarized in Section IV.

II. MODELING OF TOWER SHADOW EFFECT IN DOWNWIND WIND TURBINES

In small wind turbine application, two types of towers are commonly used to support the nacelle and the wind turbine blades. These are the tubular tower and four-leg tower, respectively. In this section, the modeling of tubular and four-leg tower shadow profiles is discussed. In particular, it is based on the Gaia-Wind's 11 kW wind turbine [20] which is configured as downwind. It is important to note that the modeling methodology presented in this work can be adapted for different types of wind turbine. The Gaia-Wind's wind turbine is chosen due to the information and hardware availability.

A. Downwind Configuration – Tubular Tower

In literature, the tower shadow effect on power quality studies was mainly focusing on the upwind wind turbine

configurations; therefore, an alternative analytical solution is sought. Reiso highlighted several steady wake models which can be used to describe the mean velocity deficit for downwind turbines; the Powles, Blevins, Schlichting, and jet wake models [21]. In 1983, Powles formulated a tower shadow model for downwind mounted rotors [22]. Through the experiments, he has found out that a cosine squared model predicted the tower shadow fairly accurately in the region of 3 - 6 tower diameters downstream [22]. Blevins' model has some similar features to Powles' model. However, it was originated from fluid dynamics which describes the wake behind a cylinder [23]. The Schlichtings' wake model originates from the boundary layer theory with the idea of a frictional surface in the interior of the flow [24]. The Powles, Blevins, Schlichting and jet wake models are simple algebraic equations which comprise of some flow dependent parameters from the downwind tower shadow, such as the wake width, velocity deficit, drag coefficient or less physical factors. These models are less computationally demanding compared to the computational fluid dynamics (CFD) simulations. The jet wake model [25] in particular will be adopted in this work as it was developed for time-series simulation. It can be implemented in Simulink and uploaded to the dSPACE controller to emulate tower shadow effect in real-time. The jet wake model has also been verified against CFD and the results can be referred in the literature [7, 25].

The jet wake model [25] was established to represent a quasi-steady reference for the time varying CFD wake velocity behind a cylindrical tower. This model is based on the boundary layer solution for a jet flowing into a fluid at rest [25]. The axial and lateral velocity components are developed as:

$$u(x,\eta) = \frac{\sqrt{3}}{2}\sqrt{\frac{K\sigma}{x}}(1 - tanh^2(\eta)) \tag{1}$$

$$v(x,\eta) = \frac{\sqrt{3}}{4}\sqrt{\frac{K\sigma}{x}}(2\eta(1 - tanh^2(\eta) - \tanh(\eta)) \tag{2}$$

where $\eta = \sigma\frac{y}{x}$, x and y are non-dimensional (with respect to tower radius) Cartesian co-ordinates in the tower cross section, as demonstrated in Fig. 1.

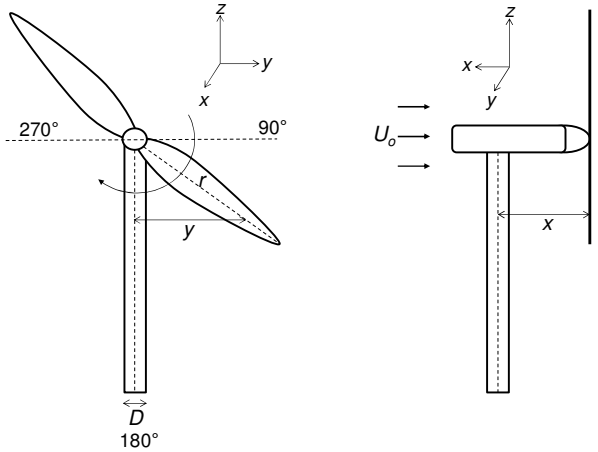

Fig. 1. Dimensions used in jet wake tower shadow formula

σ is an empirical constant equal to 7.67 [25]. K is the kinematic momentum defined as:

$$K = \frac{J_\mathrm{m}}{\rho} \tag{3}$$

where:

ρ: Air density (kg/m^3)

J_m: momentum deficit behind the tower

The derived J_m expression [25] in terms of tower parameters can be written as:

$$J_\mathrm{m} = \frac{U_0^2 D}{2}\frac{\rho}{\pi}\left[\frac{1}{8} + \frac{16}{3\pi}\right]C_\mathrm{d}^2 \tag{4}$$

where:

D: Tower diameter (m)

U_0^2: Free stream velocity (m/s)

C_d: Drag coefficient of the tower

To ease the implementation of time-series simulation, equation (1) can be converted from a function of y (lateral distance) to a function of r (radial distance) and θ (azimuthal angle) as follows:

$$u(x,r,\theta) = \frac{\sqrt{3}}{2}\sqrt{\frac{K\sigma}{x}}(1 - tanh^2\left(\sigma\frac{r\sin\theta}{x}\right)) \tag{5}$$

It should be noted that this equation only valid for $90° \leq \theta \leq 270°$. Above the horizontal, the tower shadow effects should be absent.

Using the Gaia wind turbine dimensions obtained from [26] and the parameter values as tabulated in Table 1, a simulation was performed to compare tower shadow profiles at different blade elements from the tower midline. The tower shadow profile was evaluated at radii 1 m from the hub, all the way to the tip of the blade (6.5 m) with an increment distance of 0.5 m, as shown in Fig. 2. It is observed that the blade elements closer to the hub experience tower shadow effect for a longer period. However, the wind deficit which corresponds to about 27% drop in magnitude was the same when the blade was pointing downward (180°). For all other wind speeds, a drop of 27% is also observed at an azimuthal angle of 180°. A similar tower shadow profile is observed for the upwind counterpart [10]. However, the wind deficit is 8% for the upwind case when the azimuthal angle is 180°. The simulated wind speed deficits from this work are comparable to the

TABLE I
GAIA WIND TURBINE PARAMETERS FOR TOWER SHADOW COMPUTATIONS

Parameters	Values
Undisturbed wind speed, U_0	8 m/s
Blade radius, R	6.5 m
Hub height	18 m
Tower type	Tubular
Air density, ρ (kg/m^3)	1.225
Tower drag coefficient, C_d	0.4
Tower diameter, D	0.8 m
Distance from the blade to tower midline, x	3.0 m
Sigma, σ	7.67

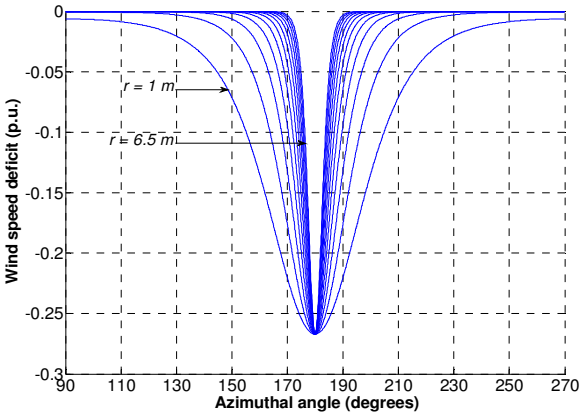

Fig. 2. Comparison of downwind tower shadow profiles at different radii from the tower midline

literature [6], which were performed using a high-fidelity CFD analysis.

Fig. 3 shows the tower shadow profiles with different longitudinal distances between the tower and the blades. As expected, the wind speed deficit is less pronounced when the blades are further away (larger *x*) from the tower. This is due to the larger allowable distance for the airflow to accelerate after being blocked by the tower. On the other hand, if the rotor plane is located closer to the tower, the influence of tower shadow effect is more severe, as demonstrated in Fig. 3. In this case, the tower clearance was varied from 1 m to 10 m. It is noticed that the tower shadow effect reduces algebraically while the tower clearance was increased linearly. The tower clearance increment from 1 m to 2 m is more efficient in reducing the tower shadow effect than increasing the tower clearance from 9 m to 10 m. Since a much higher tower clearance is needed to reduce the tower shadow effect, it is often not a viable solution as additional cost would be incurred. This is due to the requirement of a stronger material for the tower construction to support a higher moment or loading as a result of the larger tower clearance. In [7], the influence of tower clearance on tower shadow effects was investigated based on the standard downwind configuration. The authors found that an increase in tower distance from 10 m to 13.44 m resulted in a 4% decrease in tower shadow magnitude. The small decline indicates that it is not feasible to

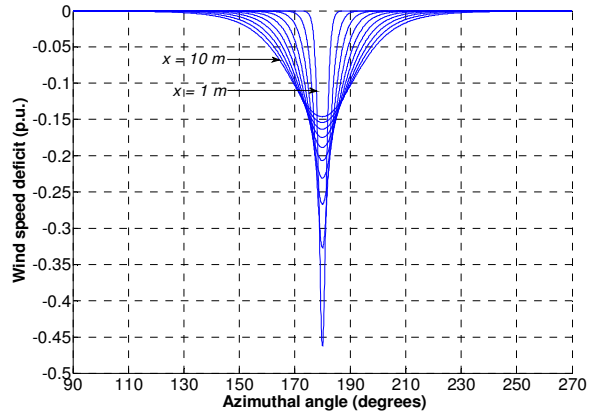

Fig. 3. Comparison of tower shadow profiles with different distances between the tower and the blades

Fig. 4. Gaia wind turbine with lattice tower configuration

reduce tower shadow effects with such approach [7]. Another promising approach to reduce the tower shadow effect may be achieved by reducing the drag coefficient of the tower by using a different build material. Again, this may incur additional cost and an economic analysis will be required to justify its advantages. Furthermore, the unsteady vortex shedding can be reduced by streamlining the body into an aerofoil shape in order to make a downwind concept viable [7]. However, it is beyond of the scope of this work to perform these studies.

B. Downwind Configuration – Four-leg Tower

An alternative tower configuration for small wind turbines is the four leg tower (also known as a lattice tower), which is connected by diagonal beams. An illustration of the Gaia wind turbine with this tower configuration is shown Fig. 4. For simplification purposes and in two-dimensional, only the four main legs are considered in this work, although the diagonal beams are likely to contribute to the wind deficit and cause unsteadiness of the flow [7]. In addition, each leg is assumed to be cylindrical in shape. The authors in [7] have performed CFD simulations on the axial wind velocity for the tubular and four-leg tower configurations. With these assumptions, the jet wake model described above was programmed in Simulink and it is used to estimate the tower shadow profile of the four-leg tower.

As the Gaia downwind wind turbine simply utilizes free-yaw mechanism, it moves freely around the tower according to the wind directions. As a result, different tower shadow profiles will be experienced due to various yaw angles relative to the rotor plane. In this work, three orientations of the tower with respect to the rotor plane are considered. These include 0°, 22.5°and 45°, respectively. Fig. 5 shows the top view of the wind turbine with three different orientations. The estimated Gaia wind turbine lattice tower dimension is shown in Fig. 5 (a). The distance between each leg is approximated as 1.2 m. Each leg is represented as a cylindrical shape with a diameter of 0.2 m. To ease the comparison between tubular

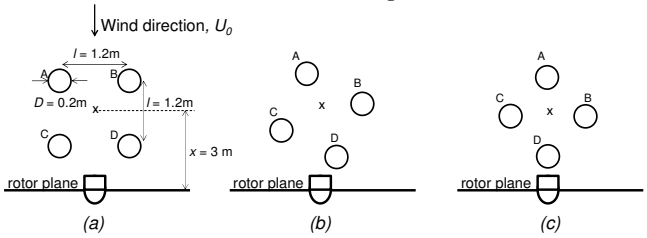

Fig. 5. Four-leg configuration with a) 0º orientation b) 22.5º orientation and c) 45 º orientation relative to the rotor plane

and lattice tower, the distance between the center of the lattice tower and the rotor plane is set as 3 m. Fig. 5 (b) and (c) show the tower orientations of 22.5°and 45°, respectively.

Using the illustrated dimensions in Fig. 5 (a), the dimensions for the case of 22.5° and 45° orientations can be easily derived from geometry. The jet wake model is utilized to estimate the wind deficit caused by each leg, at 70% radius blade section. At 70% radius of the blade section, half of the rotor area is beyond this radius and half is within. Therefore, the velocity profile is represented. The simulated tower shadow profiles for these orientations are shown in Fig. 6. Intuitively, the analytically formulated tower shadow profiles capture the qualitative behaviour for all three tower orientations. The tubular tower shadow profile is demonstrated for comparison purposes.

The 0° lattice configuration (Fig. 6 (b)) produces a narrower width of wind deficits than the tubular configuration due to the smaller leg diameter. At 0° lattice orientation, the two legs in upwind (A & B) were positioned in-line with the other two legs at downwind. The wind speed deficit due to the front legs is further reduced by the second leg. Therefore, an accumulation of wind speed deficit was experienced when the blade passes these legs. Two wind speed dips of the tower shadow profile were encountered by the blade (Fig. 6 (b)) as it rotated from position 90° to 270° (refer to Fig. 1). At 180°, the wind speed experienced by the blade recovered to the maximum value before moving towards to the next leg. Similar explanations can be used for the 22.5° and 45° orientations. The maximum wind speed deficit for these orientations occurred when the blade passes through leg D (Fig. 5 (b) & (c)). This can be attributed to the shortest distance between the leg D and the rotor plane compared to other legs. In addition, at 45° orientation, two legs (A & D) were positioned in-line with the direction of the wind. Therefore, an accumulation of wind speed deficit was experienced when the blade passes these legs at 180°.

The corresponding Fast Fourier Transform (FFT) analysis as shown in Fig. 7 reveals the harmonics contents exist within these tower shadow profiles. The FFT was performed with the simulated tower shadow profiles for 10 s. Since the rotational

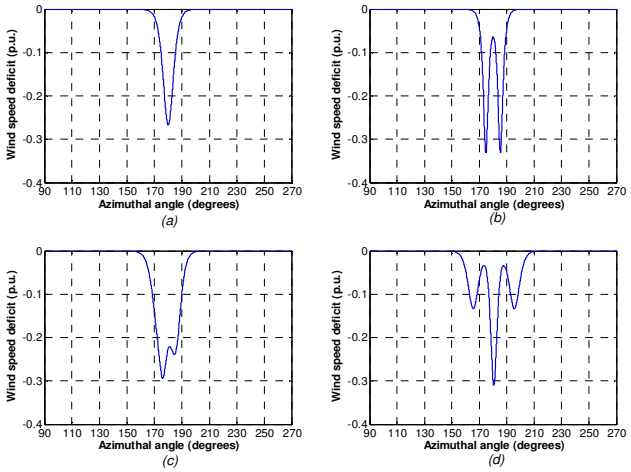

Fig. 6. Analytically derived downwind tower shadow profiles with l = 1.2 m for a) tubular tower b) four-leg 0° orientation c) four-leg 22.5° orientation d) four-leg 45° orientation to the tower

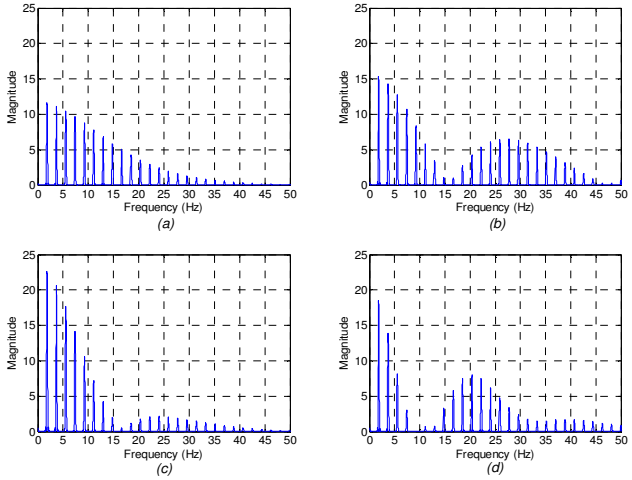

Fig. 7. FFT analysis on the tower shadow profile of a) tubular tower b) four-leg 0° orientation c) four-leg 22.5° orientation d) four-leg 45° orientation

speed of the two-bladed wind turbine is approximately 55.6 rpm, the tower shadow profile was generated at a rate of about 1.85 Hz. Therefore, the first peak of each plot corresponds to the fundamental frequency of the tower shadow profile, which is 1.85 Hz. It is important to note that the harmonic frequencies are independent of wind speed. The formula which relates the rotational speed of the wind turbine blades and the fundamental frequency (in hertz) of the tower shadow profile is given as:

$$f_1 = \frac{m}{60} \times n \tag{6}$$

where:

m: Rotational speed of the wind turbine (rpm)

n: Number of blades

The magnitude of the higher order harmonics is dependent on the generated tower shadow profiles, which varies with tower structures.

For the case of tubular tower (Fig. 7 (a)), the harmonics decrease algebraically in magnitude. These plots further indicate that the representation of tower shadow using a sinusoidal waveform in the past [18, 19] is oversimplified. For the case of lattice tower configuration, the harmonics profile is dependent on its orientation against the wind direction. For 0° and 45° orientations, the high-frequency harmonics are more apparent. This is also reflected from the time-series profile from Fig. 6. It can be visualized that the lattice configuration generates a more sophisticated tower shadow profile at varying degrees of orientation, compared to its tubular counterpart.

III. Characterization of Tower Shadow Profile Using a Wind Turbine Emulator

This section describes the characteristics and limitations of the tower shadow profile generated from the wind turbine emulator, which was set up as part of a hybrid system in the laboratory. The overall block diagram of the hybrid system is shown in Fig. 8 and their corresponding components are shown in Fig. 9.

Three single-phase Sunny Island (SI) inverters were used to form an isolated three-phase grid with energy being supplied from the Rolls batteries, which have the total capacity of 106

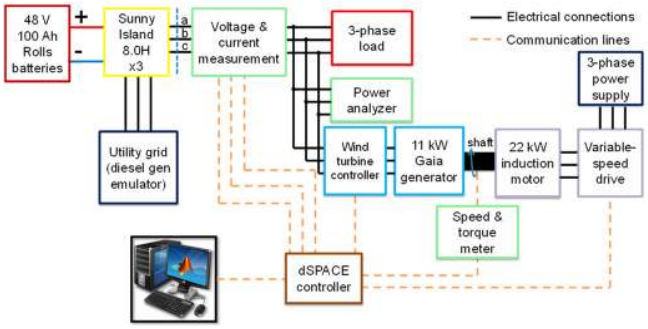

Fig. 8. Off-grid wind turbine emulator laboratory setup

Fig. 9. Hybrid system lab setup equipment

Ah. In reality, the Gaia Ltd's 133-11 kW fixed speed wind turbine consists of 4 main components: the blades, the step-up gearbox, the induction generator and the wind turbine controller. The induction generator was connected to the isolated grid via a wind turbine controller. While the aerodynamics and inertia of the blade and gearbox were programmed in dSPACE, the 11 kW generator's inertia effect on generating the tower shadow profile was taken into consideration as the system is not scaled down. In this work, a 22 kW induction motor was used to emulate the wind energy to drive the induction generator. The motor was driven by a variable-speed AC drive (Parker SSD Drive). The SSD drive is capable of controlling the motor with two control topologies; speed control and torque control. As the Gaia wind turbine is a fixed speed wind turbine, torque control topology of the SSD drive was adopted in driving the 22 kW induction motor. With the generator running at a near-constant speed, the torque can be controlled to emulate the varying mechanical torque input due to varying wind speeds. The torque input was fed through a dSPACE DS1103 controller. By programming different torque demand at the inverter drive, the tower shadow effect which causes a reduction in wind speed was modeled. In addition, the aerodynamics of the blade and gearbox were modeled in Simulink. A load bank is connected in parallel with the induction generator output.

The ControlDesk is a software program which acts as an interface between the Simulink and the dSPACE controller. The implemented ControlDesk front panel interface for the test rig application is shown in Fig. 10. It allows user to control and monitor the test rig in real time. These include varying the mean wind speed, tower shadow profiles and observing the corresponding voltage, current, frequency and

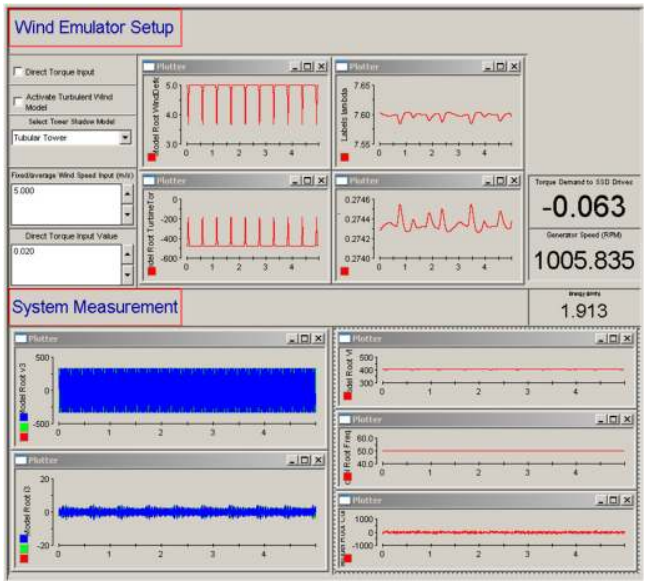

Fig. 10. ControlDesk front panel

power waveforms. The steady-state and dynamic analysis of the standalone hybrid system is presented in [27].

Within the test rig, an induction motor was used to emulate the wind speed experienced by the blades of the wind turbine. Since this wind speed takes into consideration of the tower shadow effect, it is important to investigate the frequency response of the induction motor. As highlighted earlier, for the case of Gaia wind turbine, the tubular tower can cause a wind speed deficit of about 27%. In addition, the wind speed deficit takes a short period to recover to the nominal wind speed level, usually in the order of hundreds of milliseconds. Fig. 11 shows the block diagram with the designated measuring points throughout the characterization process.

The test was carried out with an input wind speed of 8 m/s, together with the tower shadow profile shown in Fig. 12 (a). In order to avoid high charging current on the batteries, a three-phase load of 7 kW was switched-on to absorb the power generated from the 11 kW induction machine. The corresponding torque demand for the variable speed drive is depicted in Fig. 12 (b). The torque and speed which were measured at the shaft are shown in Fig. 12 (c) and (d), respectively. The rotational speed sampling rate was limited by the speed & torque meter, which in this case it was 0.1 s. It is noticed that an oscillation occurred on the torque profile during the transition to steady-state. This recovery took place for about 1.5 s. It was an undesirable scenario as the torque fluctuations have exceeded the machine's full-load torque. It is known that when an induction machine operates beyond its

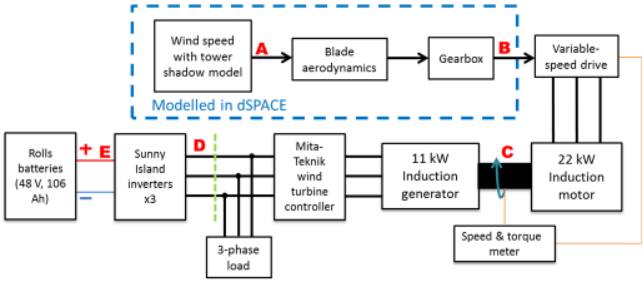

Fig. 11. Block diagram of wind turbine emulator setup with the highlighted measurement points

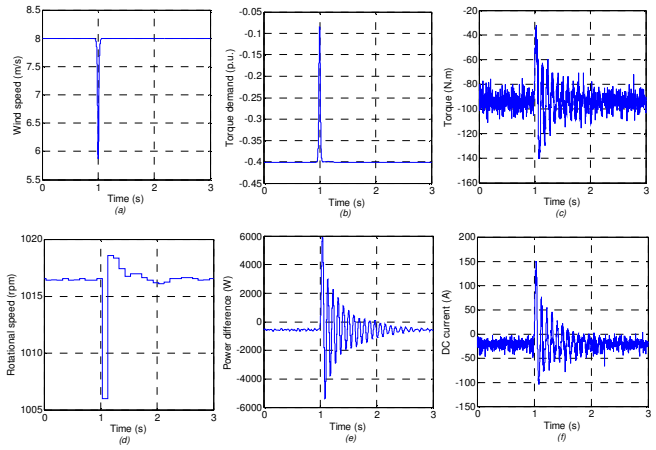

Fig. 12. a) Point A – simulated wind speed experienced by the blade with tower shadow profile b) Point B – simulated torque demand on the variable speed drive. Measurement results at various stages of the test rig c) Point C – measured torque at the shaft d) Point C – measured rotational speed at the shaft e) Point D – measured power at the terminals of the induction generator f) Point E – batteries DC current flow

full-load region, the leakage flux becomes dominant and this induces high reactive power. As a result, the machine would be operated at low power factor. Fig. 12 (e) shows the measured power at point D of Fig. 11. This power corresponds to the difference between the generated power from the 11 kW machine and the constant load demand. However, the focus here is to analyze the power output profile. As expected, the oscillation from the shaft was propagated to the power output produced by the generator. The high magnitude power oscillations can cause additional thermal stress on the windings and iron core laminations of the machine. Eventually, the machine may fail. Finally, the battery current profile (Fig. 12 (f)) which was measured at point E, possessed similar transients compared to the power output of the generator. High power losses and thermal stresses were imposed on the batteries due to the existence of internal resistances.

An FFT analysis was performed (shown in Fig. 13) on the power output (Fig. 12(e)) in order to analyze the frequency contents of the oscillation. The peak magnitude of the oscillation was identified to be located at just below 11 Hz. Analyzing the tubular tower shadow FFT profile (Fig. 7 (a)), it

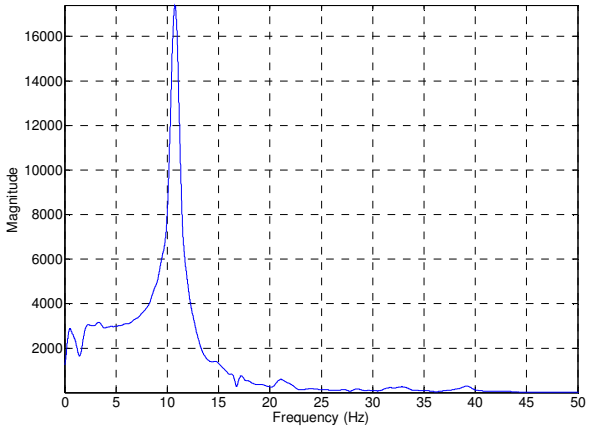

Fig. 13. FFT analysis of the emulated tower shadow power transient

is noticed that the fifth harmonic of the fundamental frequency coincides with the oscillation frequency of the output power. Hence, it can be concluded that the induction motor drive system is highly responsive to this frequency input.

A simplified test on the system frequency response was designed and being carried out in order to verify the hypothesis mentioned above. In the proposed test, the wind speed (input to the system) was formulated as a sinusoidal waveform with a mean wind speed of 5 m/s and amplitude of 0.5 m/s. This causes the torque demand of the variable-speed drive to vary accordingly, which further propagate along the shaft and finally seen by the generator. Therefore, it is expected that the generator would respond to these variations by producing fluctuated power output. The test was carried out with frequencies of 7 Hz, 9 Hz, 11 Hz, 13 Hz, 15 Hz and 20 Hz. While performing these tests, a constant resistive load which was connected in parallel with the generator was switched on, thus allowing the power variations to be observed at zero-crossings. The measured torque at the shaft and the net power differences between the 11 kW generator and the load are shown in Fig. 14 – 19. In these figures, it can be observed that the measured shaft torque was experiencing sustained oscillations, with its magnitude increasing as the frequency increased from 7 Hz to 9 Hz. Another test was

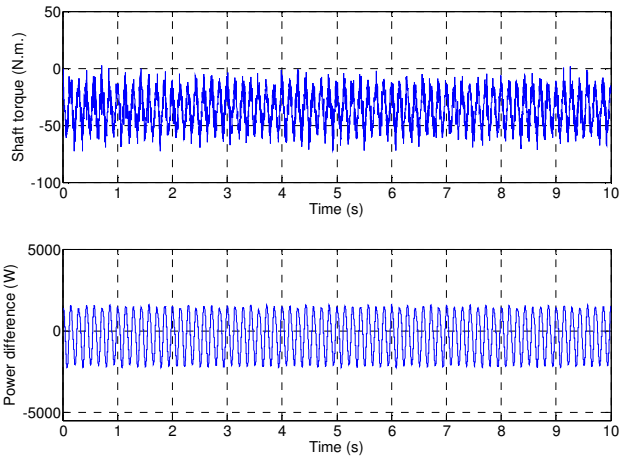

Fig. 14. Measurement of the torque at shaft and the power difference between the generator and the load with a 7 Hz of wind speed input.

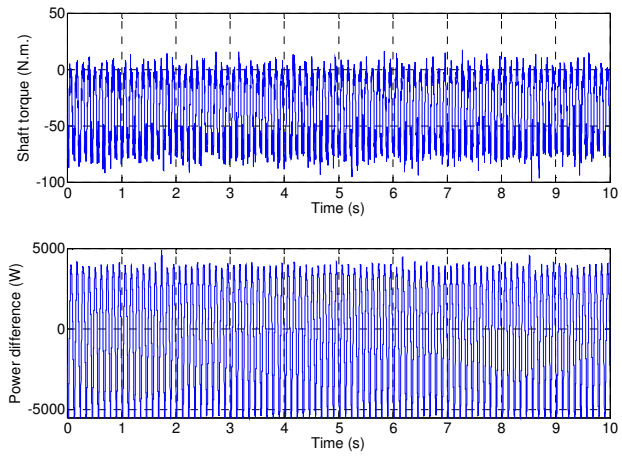

Fig. 15. Measurement of the torque at shaft and the power difference between the generator and the load with a 9 Hz of wind speed input.

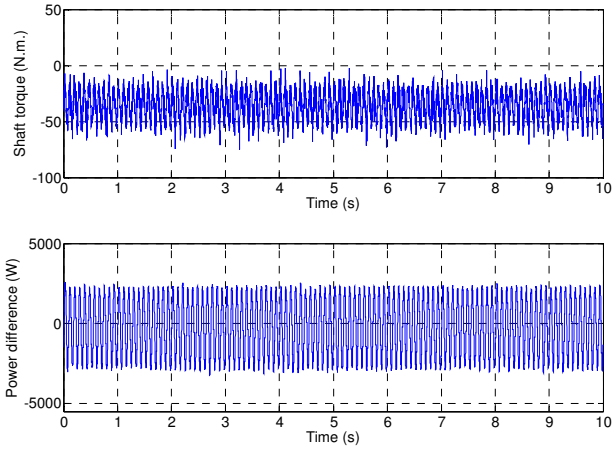

Fig. 16. Measurement of the torque at shaft and the power difference between the generator and the load with an 11 Hz of wind speed input.

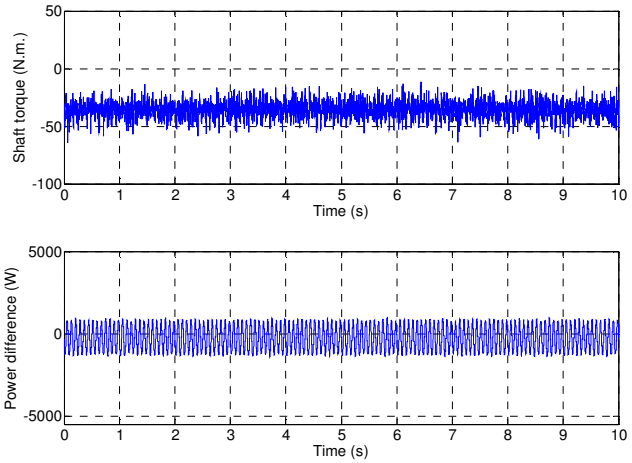

Fig. 17. Measurement of the torque at shaft and the power difference between the generator and the load with a 13 Hz of wind speed input.

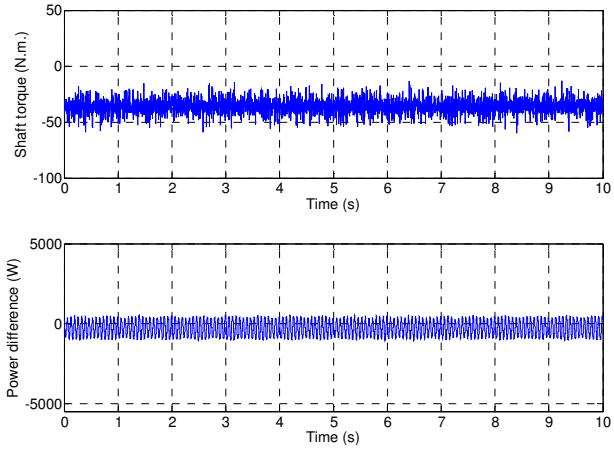

Fig. 18. Measurement of the torque at shaft and the power difference between the generator and the load with a 15 Hz of wind speed input.

conducted with an input frequency of 10 Hz and the results are shown in Fig. 20. At this frequency, the induction machine drive system became unstable at approximately 7.8 second. The rotational speed accelerated and the system tripped at about 8.5 second. The load demand (constant power) is fully supplied by the grid-forming inverter system as soon as the generator became unstable (acceleration began). However, the

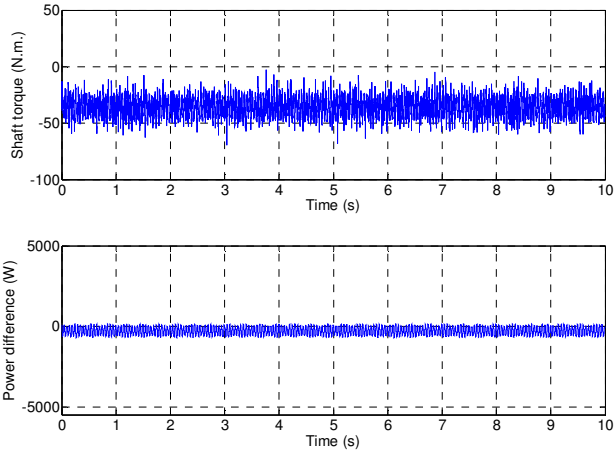

Fig. 19. Measurement of the torque at shaft and the power difference between the generator and the load with a 20 Hz of wind speed input.

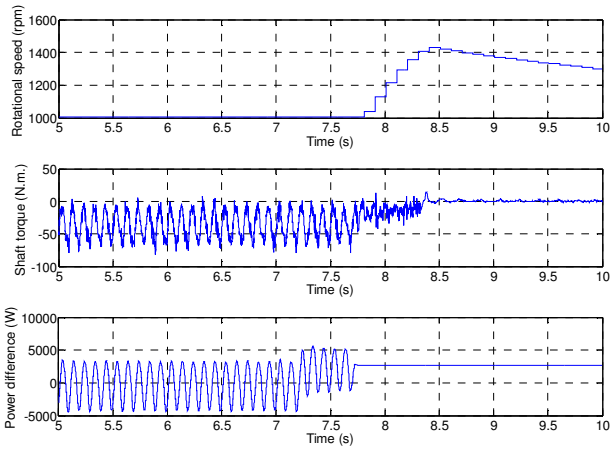

Fig. 20. Measurement of the shaft rotational speed, torque and the power difference between the generator and the load with a 10 Hz of wind speed input. Unstable operation began at approximately 7.7 s

oscillation decreases (as shown in Fig. 15 – 19) with the input frequency increases. This can be observed when the input frequency was set to 11 Hz, 13 Hz, 15 Hz and 20 Hz, respectively.

The stability problem in the induction motor drive systems have been studied in the past [28, 29]. Authors in [28, 29] highlighted that the stability problem can be viewed from the interactions between the electric transients and the rotor dynamics. The oscillatory behavior of the system can be directly linked with the existence of the winding resistances and leakage inductances. In real machine with losses, it was mentioned that a stability problem will not occur if the electromagnetic torque is precisely controlled at the desired value required from the load side. In addition, the unstable phenomena (also known as hunting phenomena) can be associated with the variation of slip frequency. This undesirable rotor motion also leads to a phase angle variation of the magnetic flux in the air-gap. Even under a constant rotor speed circumstance, the abrupt variation of the stator voltage or current not accompanied by right control of the air-gap flux can cause oscillation [28]. Literature [28] has also simulated a scenario whereby the fluctuations of rotor speed can cause nonlinear and parametric oscillation within the

system. When the real part of a dominant eigenvalue becomes positive, the system will be in an unstable state, as demonstrated by the case of 10 Hz input frequency in this work. Moving beyond 11 Hz cases, the decay in oscillation magnitudes can be attributed to the slower response time of the machine due to its inertia. The machine can be seen as a "low pass filter", therefore has a little reaction against the high-frequency inputs.

One way to mitigate the above-mentioned oscillation effects is through the control of rotational speed of the turbine rotor. With a carefully tuned rotational speed, it is expected that the tower shadow's harmonic frequencies would be altered accordingly. This serves as awareness for future test rig developers should such problem arises. Another method to absorb the rapid power fluctuations is to utilize short-term energy storage system. For instance, supercapacitors which can tolerate many more charge and discharge cycles than the batteries are suitable to be adopted in this application. However, a dc-dc converter with an appropriate control strategy is required to manage these fluctuations effectively.

In order to further understand the test rig's characteristics with respect to the modeled tower shadow profiles, two sensitivity analyses were carried out. The impact of tower shadow's widths and its magnitude on the oscillations were studied respectively. Since the purpose of this test was to observe the generator output power profile given an input tower shadow profile, only the wind speed with tower shadow profile and its corresponding output power are shown in the following.

The study on different tower shadow widths and their corresponding oscillating power output are shown in Fig. 21. By considering the tower shadow experienced at different blade sections, various tower shadow widths of the same magnitude can be obtained. As expected, the tower shadow profile experienced by the blade section closer to the hub has a wider width compared to the sections near the tip. From the measured output power profiles, it can be concluded that the tower shadow profile with a wider width contributes to a higher oscillation magnitude compared to the smaller width counterpart, despite having the same peak magnitude of tower shadow. However, it can be seen that the oscillation frequency is the same for all cases and they decay at the same rate.

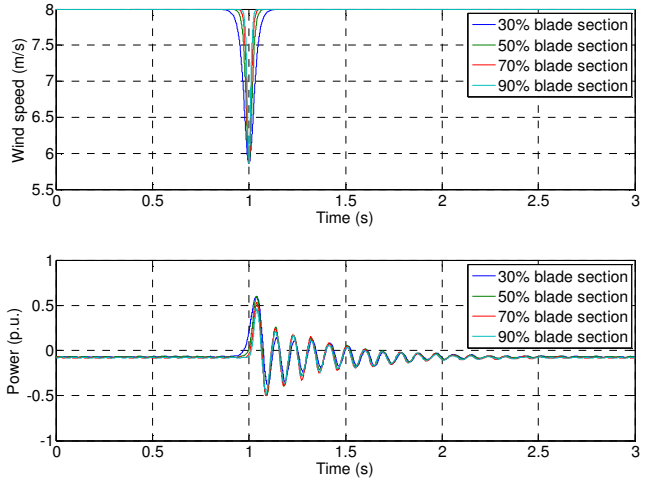

Fig. 21. Sensitivity analysis on the tower shadow widths against the power oscillations

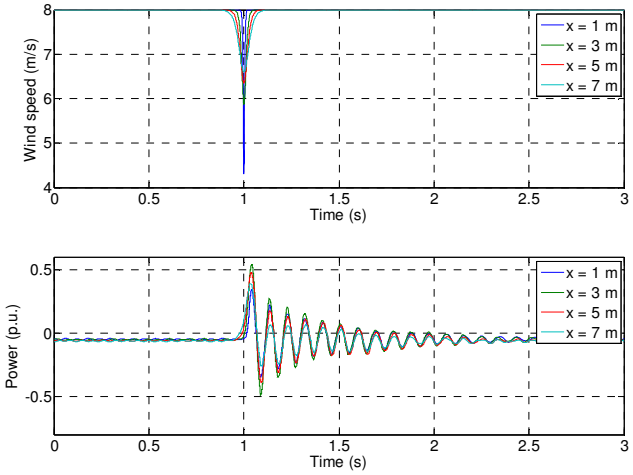

Fig. 22. Sensitivity analysis on the tower shadow magnitudes against the power oscillations

Next, the power oscillations due to different tower shadow magnitudes are shown in Fig. 22. In this case, the tower shadow profiles were generated by varying the distance between the center of the tower and the rotor plane, x. Note that the width of the profile changes as the distance between the tower and the rotor plane was varied. Interestingly, the highest magnitude of tower shadow (smallest width) did not produce the highest oscillations. This can be attributed to the very small width of the tower shadow profile, where the energy of the high-frequency components is "not seen" by the induction motor drive system. As the distance, x moved from 3 m to 5 m, the tower shadow magnitude was reducing and this was being reflected accordingly at the generator power output. Therefore, this test further highlighted another limitation of the induction machine drive system in responding the tower shadow profiles which have relatively small widths.

IV. Conclusion

In conclusion, this paper has analyzed the tower shadow modeling of the downwind wind turbine. The limitations of emulating tower shadow using wind turbine emulators are highlighted. The cause of the torque oscillations, which was generated from the wind turbine emulator was identified and discussed. The torque oscillation frequency is unique and it is dependent on the stability characteristics of the induction motor drive system used. This paper has contributed the methodology of characterizing the oscillations, which was demonstrated experimentally. In particular, the research also highlighted the importance of these test methods from the tower shadow emulation point of view. The characteristics of tower shadow profiles from both tubular and lattice towers are clearly demonstrated. The finding here is important for future wind energy conversion system test rig designers as they serve as additional considerations while designing wind turbine emulator in the laboratory.

REFERENCES

[1] "World Energy Outlook 2014 Factsheet," *International Energy Agency (IEA)*, Paris, France.

[2] T. Ackermann, *Wind Power in Power Systems*, 2nd ed.: Wiley-Blackwell, 2012.

[3] A. Arulampalam, M. Barnes, N. Jenkins, and J. B. Ekanayake, "Power quality and stability improvement of a wind farm using STATCOM supported with hybrid battery energy storage," *IEE Proceedings - Generation, Transmission and Distribution,* vol. 153, pp. 701-710, 2006.

[4] A. Tummala, R. K. Velamati, D. K. Sinha, V. Indraja, and V. H. Krishna, "A review on small scale wind turbines," *Renewable and Sustainable Energy Reviews,* vol. 56, pp. 1351-1371, 2016.

[5] J. F. Manwell, J. G. McGowan, and A. L. Rogers, *Wind Energy Explained: Theory, Design and Application*: Wiley-Blackwell, 2009.

[6] Q. Y. Zhao, C. H. Sheng, and A. Afjeh, "Computational Aerodynamic Analysis of Offshore Upwind and Downwind Turbines," *Journal of Aerodynamics,* vol. 2014, p. 13, 2014.

[7] F. Zahle, H. A. Madsen, and N. N. Sørensen, "Research in Aeroelasticity EFP-2007-II," *Danmarks Tekniske Universitet, Risø Nationallaboratoriet for Bæredygtig Energi.*

[8] D. McSwiggan, T. Littler, D. J. Morrow, and J. Kennedy, "A study of tower shadow effect on fixed-speed wind turbines," in *43rd International Universities Power Engineering Conference (UPEC)*, 2008, pp. 1-5.

[9] A. Lazkano, K. Redondo, P. Saiz, J. J. Gutierrez, I. Azcarate, L. A. Leturiondo, and J. Barros, "Case study: Flicker emission and 3P power oscillations on fixed-speed wind turbines," in *15th IEEE International Conference on Harmonics and Quality of Power (ICHQP)*, 2012, pp. 268-273.

[10] D. S. L. Dolan and P. W. Lehn, "Simulation model of wind turbine 3p torque oscillations due to wind shear and tower shadow," *IEEE Transactions on Energy Conversion,* vol. 21, pp. 717-724, 2006.

[11] P. Sørensen, A. D. Hansen, and P. A. C. Rosas, "Wind models for simulation of power fluctuations from wind farms," *Journal of Wind Engineering and Industrial Aerodynamics,* vol. 90, pp. 1381-1402, 2002.

[12] J. D. M. De Kooning, T. L. Vandoorn, J. Van de Vyver, B. Meersman, and L. Vandevelde, "Shaft speed ripples in wind turbines caused by tower shadow and wind shear," *IET Renewable Power Generation,* vol. 8, pp. 195-202, 2014.

[13] H. Weihao, S. Chi, and C. Zhe, "Impact of wind shear and tower shadow effects on power system with large scale wind power penetration," in *37th Annual Conference on IEEE Industrial Electronics Society (IECON)*, 2011, pp. 878-883.

[14] J. Tan, W. Hu, X. Wang, and Z. Chen, "Effect of Tower Shadow and Wind Shear in a Wind Farm on AC Tie-Line Power Oscillations of Interconnected Power Systems," *Energies,* vol. 6, p. 6352, 2013.

[15] J. M. Nye, J. G. de la Bat, M. A. Khan, and P. Barendse, "Design and implementation of a variable speed wind turbine emulator," in *International Conference on Electrical Machines (ICEM)*, 2012, pp. 2060-2065.

[16] S. Wan, L. Cheng, and X. Sheng, "Effects of Yaw Error on Wind Turbine Running Characteristics Based on the Equivalent Wind Speed Model," *Energies,* vol. 8, p. 6286, 2015.

[17] R. Fadaeinedjad, G. Moschopoulos, and M. Moallem, "The Impact of Tower Shadow, Yaw Error, and Wind Shears on Power Quality in a Wind-Diesel System," *IEEE Transactions on Energy Conversion,* vol. 24, pp. 102-111, 2009.

[18] E. Sakasegawa, K. Shinohara, K. Yamamoto, and M. Hombu, "Characteristic analysis of a wind power system with doubly fed induction generator in considering of the tower shadow effect," in *International Power Electronics Conference (IPEC)*, 2010, pp. 3225-3229.

[19] A. G. Abo-Khalil, "A new wind turbine simulator using a squirrel-cage motor for wind power generation systems," in *IEEE Ninth International Conference on Power Electronics and Drive Systems (PEDS)*, 2011, pp. 750-755.

[20] "User Manual - Gaia-Wind 11 kW Turbine," *Gaia-Wind Ltd.*, United Kingdom, August 2008.

[21] M. Reiso, "The Tower Shadow Effect in Downwind Wind Turbines," PhD Thesis, Department of Civil and Transport Engineering, Norwegian University of Science and Technology (NTNU), Norway, May 2013.

[22] S. R. J. Powles, "The effects of tower shadow on the dynamics of a horizontal axis wind turbine," *Wind Engineering,* vol. 7, pp. 26-42, 1983.

[23] R. D. Blevins, *Flow-Induced Vibrations*. New York: Van Nostrand Reinhold, 1990.

[24] H. Schlichting and K. Gersten, *Boundary-Layer Theory*. Berlin: Springer, 2000.

[25] H. A. Madsen, J. Johansen, N. N. Sørensen, G. C. Larsen, and M. H. Hansen, "Simulation of low frequency noise from a downwind wind turbine rotor," in *45th AIAA Aerospace Sciences Meeting and Exhibit*, pp. 1-12, 2007.

[26] M. Molinari, M. Pozzi, D. Zonta, and L. Battisti, "In-field testing of a steel wind turbine tower," in *International Modal Analysis Conference (IMAC) XXVIII*, Florida USA, 2010.

[27] L. K. Gan, J. K. H. Shek, and M. A. Mueller, "Modelling and experimentation of grid-forming inverters for standalone hybrid wind-battery systems," in *2015 International Conference on Renewable Energy Research and Applications (ICRERA)*, 2015, pp. 449-454.

[28] K. Koga, R. Ueda, and T. Sonoda, "Stability problem in induction motor drive system," in *IEEE Industry Applications Society Annual Meeting*, 1988, pp. 129-136.

[29] R. Ueda, T. Sonoda, K. Koga, and M. Ichikawa, "Stability analysis in induction motor driven by v/f controlled general-purpose inverter," *IEEE Transactions on Industry Applications,* vol. 28, pp. 472-481, 1992.

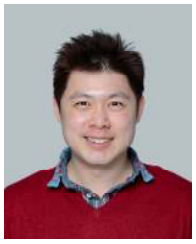

Leong Kit Gan received the B.Eng. of Electrical & Electronics Engineering (Hons.) from the Universiti Tenaga Nasional, Kuala Lumpur, Malaysia, in 2009. In 2012, he graduated with M.Sc. in Sustainable Energy Systems from The University of Edinburgh, Edinburgh, U.K. From 2012 to 2016, he pursued his Ph.D. degree in Energy Systems at The University of Edinburgh, Edinburgh, U.K.

From 2009 to 2011, he was an Electronics Engineer in Altera and Motorola. Currently, he is a Postdoctoral Researcher at the University of Oxford, Oxford, U.K., focusing on intelligent energy management systems and modeling of flow batteries.

His research interests include power electronics, energy storage systems, renewable energy systems, control and optimization.

Jonathan K. H. Shek received the M.Eng. (Hons.) and the Ph.D. degrees from The University of Edinburgh, U.K., in 2004 and 2009, respectively.

From 2009 to 2012, he was a Postdoctoral Researcher working in the area of power take-off, condition monitoring, and control for renewable energy devices. His research interests include power electronics and control, particularly its application in sustainable energy systems, such as renewable energy and electric vehicles.

Dr. Shek currently holds the position of Chancellor's Fellow with the Institute for Energy Systems at The University of Edinburgh.

Markus A. Mueller graduated with a B.Sc. (Eng.) in Electrical and Electronic engineering from Imperial College London, in 1988. He was awarded a PhD in Electrical Engineering from University of Cambridge in 1991.

For 3 years he worked as a Research Assistant at Cambridge working on induction motors, and then spent 2 years in industry with Brook Hansen and SR Drives Ltd. From 1997 to December 2003, he was a lecturer in the School of Engineering at the University of Durham. In January 2004 he joined the School of Engineering at the University of Edinburgh, and in August 2012 he was given a Personal Chair in Electrical Machines. He is Head of the Research Institute for Energy Systems within the School of Engineering. In 2009 he founded NGenTec Ltd. to commercialise a

permanent magnet generator for wind turbines. His research interests include the design and modeling of electrical machines for renewable energy converters.